

Review

## Fischer-Tropsch Synthesis on Multicomponent Catalysts: What Can We Learn from Computer Simulations?

José L. C. Fajín <sup>1,\*</sup>, M. Natália D. S. Cordeiro <sup>1</sup> and José R. B. Gomes <sup>2</sup>

<sup>1</sup> REQUIMTE, Departamento de Química e Bioquímica, Faculdade de Ciências, Universidade do Porto, P-4169-007 Porto, Portugal; E-Mail: ncordeir@fc.up.pt

<sup>2</sup> CICECO, Departamento de Química, Universidade de Aveiro, 3810-193 Aveiro, Portugal; E-Mail: jrgomes@ua.pt

\* Author to whom correspondence should be addressed; E-Mail: jfajin@fc.up.pt; Tel.: +351-220-402-552; Fax: +351-220-402-659.

Academic Editor: Keith Hohn

Received: 28 November 2014 / Accepted: 24 December 2014 / Published: 9 January 2015

---

**Abstract:** In this concise review paper, we will address recent studies based on the generalized-gradient approximation (GGA) of the density functional theory (DFT) and on the periodic slab approach devoted to the understanding of the Fischer-Tropsch synthesis process on transition metal catalysts. As it will be seen, this computational combination arises as a very adequate strategy for the study of the reaction mechanisms on transition metal surfaces under well-controlled conditions and allows separating the influence of different parameters, e.g., catalyst surface morphology and coverage, influence of co-adsorbates, among others, in the global catalytic processes. In fact, the computational studies can now compete with research employing modern experimental techniques since very efficient parallel computer codes and powerful computers enable the investigation of more realistic molecular systems in terms of size and composition and to explore the complexity of the potential energy surfaces connecting reactants, to intermediates, to products of reaction. In the case of the Fischer-Tropsch process, the calculations were used to complement experimental work and to clarify the reaction mechanisms on different catalyst models, as well as the influence of additional components and co-adsorbate species in catalyst activity and selectivity.

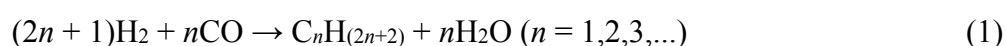
**Keywords:** Fischer-Tropsch synthesis; density functional theory; multicomponent catalysts

---

## 1. Introduction

The Fischer-Tropsch synthesis is a chemical process discovered by the chemists Franz Fischer and Hans Tropsch in the nineteen-twenties [1]. The main reaction of this chemical process consists in the combination of hydrogen and carbon monoxide (synthesis gas, with H<sub>2</sub>/CO ratio of ~2 that is controlled by the water gas shift reaction) on a solid catalyst to produce liquid hydrocarbons. During the Fischer-Tropsch process many different hydrocarbons, e.g., methane, alkanes, alkenes, branched alkanes, and oxygenated compounds, e.g., alcohols, aldehydes, ketones, and fatty acids, from secondary reaction routes are also produced [2–6].

In order to produce synthetic fuels, typically from coal, natural gas or biomass, the process conditions and catalyst composition are usually chosen to favor the production of hydrocarbons with a long-straight chain (>C<sub>5</sub>) and to minimize the formation of methane, olefins, branched alkanes and oxygenated species [7–11]. Thus, the route for the production of long-straight chain alkanes can be well described by the following chemical equation:



Usually, only relatively small quantities of non-alkane products are formed, although catalysts favoring some of these byproducts have been also developed [12,13].

The Fischer-Tropsch synthesis process was intensively used during the World War II period for the production of synthetic fuels from coal due to the difficulties felt by some countries to grant access to sufficient amounts of crude oil [14]. Since then, catalysts based on iron, cobalt and ruthenium metals have been the most widely used. Unfortunately, all are far from being perfect since other factors beyond activity loss due to catalyst aging (e.g., conversion of the active phase, loss of active specific surface area, fouling, *etc.*) are found to affect their performances or hamper their improvement. For instance, iron, despite being very cheap, forms many different phases, but the most active one is still unresolved; cobalt seems to be the most effective of these three transition metals but it is dramatically poisoned by sulfur species, which prevents its utilization when used with syngas from coal or biomass; and ruthenium is associated with interesting activities at low temperature but it is very expensive. Additionally, energy costs are quite large with any of the catalysts developed so far and the process becomes very interesting only in situations associated with high prices of crude oil.

Nowadays, oil reserves are decreasing quite fast, which is being accompanied by a concomitant raise of the petroleum price. Hence, many researchers are focusing their current scientific interests in the development of new catalysts for the Fischer-Tropsch synthesis [15]. Not only Fe, Co and Ru are being considered in this quest for novel catalysts for the Fischer-Tropsch synthesis reaction. Other transition metals (and alloys of different metals) are being considered, especially those from group VIIIA in the Periodic Table because they display some activity in the C–C coupling reaction during CO hydrogenation [13,16–29]. Yet, this is not a trivial task since small variations in the catalyst composition change dramatically the reaction yield and/or selectivity. For instance, the addition of Pt or Ru to Co enhances the activity of the catalyst for the Fischer-Tropsch reaction [30], but the addition of high quantities of Pt to Co based catalysts changes their selectivity toward methanol production [31].

The inclusion of other components into the traditional catalysts for the Fischer-Tropsch reaction can be used to improve the activity and selectivity of the catalyst, as for example with the addition of ionic

additives to ruthenium nanoparticles, which increases the activity and modifies the selectivity toward long-straight hydrocarbon chains, olefins or alcohols, depending on the ionic additive used [12]. Other elements can be added to the catalyst for preventing its poisoning by deposition of species like carbon [32,33] or sulfur [34]. High selectivities toward other byproducts can be also achieved by the use of promoters. For instance, the inclusion of Fe into Ni/ $\gamma$ -Al<sub>2</sub>O<sub>3</sub> is accompanied by an increase in the CO methanation [35]. The latter reaction is also enhanced when Ca, La, K, Ni and/or Co are added to a Ru/TiO<sub>2</sub> catalyst, being especially active the Ca-Ni-Ru/TiO<sub>2</sub> one [36]. The production of olefins is favored by catalysts based on Fe-Mn-V-K [37] or based on Fe-Mn nanoparticles supported on carbon nanotubes [38]. Branched hydrocarbons can be obtained from the Fischer-Tropsch synthesis on Fe-Si-K and Co/SiO<sub>2</sub> based catalysts through the alkylidene mechanism [39].

The activity and selectivity of the multicomponent catalysts are determined by the catalyst composition, but also by other factors such as the temperature [40], the oxidized/reduced level of the catalyst components, which is modulated with promoters [41–43], or the size of the catalyst particles [11,28,44,45]. Furthermore, the incorporation of different species into the catalyst (i) can modulate the catalyst activity by conferring a different microstructure to the active sites of the catalyst [46]; (ii) can establish synergic effects with preexistent phases [47] or (iii) can have a separate role from the other catalyst phases [31,48].

The examples above clearly show that our understanding on the role of each catalyst phase and on the most favorable mechanistic pathways in catalysts suggested for the Fischer-Tropsch synthesis is still in its infancy. Therefore, scientific knowledge gathered from experimental and computational studies on catalyst models working under well-controlled conditions is mandatory. Herewith, it is reviewed the literature on the application of computational methods to the study of the Fischer-Tropsch synthesis on multicomponent catalysts, in particular that with emphasis in the determination of the preferential reaction mechanisms.

## 2. Computational Studies on Catalyst Surface Models

As referred above, the addition of extra components to the traditional Fischer-Tropsch catalysts can enhance their performance by increasing the activity [30,36] and selectivity [12,31,37–39], or by avoiding catalyst poisoning [32–34]. In this section we will show how computational methods can help in the understanding of the Fischer-Tropsch catalysis by solid catalysts. In fact, computational approaches have been widely used in the study of reaction mechanisms on simple catalysts models, which are usually based on monometallic surfaces. In the case of the Fischer-Tropsch synthesis reaction, Ojeda *et al.* [19] studied through density functional theory, *cf.* Table 1, the formation of methane from CO and H<sub>2</sub> on Fe(110) and Co(0001) surfaces. Their calculations show that the reaction of direct CO bond cleavage,



where \* denotes a free site on the catalyst surface, is energetically much more expensive than the dissociation of the C–O via the hydroxymethylidyne, COH, intermediate,



and also more energetically expensive than the dissociation following the route through the formyl (HCO or oxymethylidyne) intermediate,



with energetic data summarized in Table 2. A representation of the reaction steps corresponding to the carbide, hydroxymethylidyne and formyl routes for the CO dissociation in the Fischer-Tropsch reaction can be seen in Figure 1.

**Table 1.** Computational details for the calculations devoted to the study of the Fischer-Tropsch process on transition metal surfaces that are reviewed in this article.

Code <sup>a</sup>	DFT <sup>b</sup>	Basis set <sup>c</sup>	Transition metal surface(s) <sup>d</sup>	Ref.
DACAPO	PW91	PW-USPP	Fe(110) and Co(0001)	Ojeda <i>et al.</i> [19]
DACAPO	RPBE	PW-USPP	Ru(0001) and Ru(10 $\bar{1}$ 9)	Vendelbo <i>et al.</i> [23]
VASP	PBE	PW-PAW	Co(0001), Pt@Co(0001), and Ru@Co(0001)	Balakashnan <i>et al.</i> [32]
CASTEP	PW91	PW-USPP	Pt(111), Pd(111), and Ru(0001)	Inderwildi <i>et al.</i> [49]
CASTEP	PW91	PW-USPP	Co(0001)	Inderwildi <i>et al.</i> [50]
VASP	RPBE	PW-USPP	Ru(0001)	Loveless <i>et al.</i> [51]
VASP	PW91	PW-USPP	Ru(10 $\bar{1}$ 5)	Ciobica <i>et al.</i> [52]
VASP	PBE	PW-PAW	Ru(11 $\bar{2}$ 1)	Shetty <i>et al.</i> [53]
VASP	PBE	PW-PAW	Ru(10 $\bar{1}$ 0)B and Co(10 $\bar{1}$ 0)B	Shetty <i>et al.</i> [54]
VASP	PBE	PW-PAW	Co(0001), Co(10 $\bar{1}$ 2), and Co(11 $\bar{2}$ 0)	Liu <i>et al.</i> [55]
VASP	PW91	PW-PAW	Ni(111), Ni(110), Rh@Ni(111), Rh@Ni(110), Ru@Ni(111) and Ru@Ni(110)	Fajin <i>et al.</i> [56]
Siesta	PBE	DZP-TMPP	Co(0001)	Cheng <i>et al.</i> [57]
Siesta	PBE	DZP-TMPP	Ru(001) <sup>e</sup> , Fe(210), Rh(211), and Re(001) <sup>e</sup>	Cheng <i>et al.</i> [58]
VASP	PW91	PW-PAW	Rh(111) and Rh(211)	van Grootel <i>et al.</i> [59]
SeqQuest	PBE	DZP-TMPP	Ni(111)	Mueller <i>et al.</i> [60]
-	GGA	PW-USPP	Rh(111)	Zhang <i>et al.</i> [61]
VASP	PW91	PW-PAW	Rh(111), Ni(111), and Rh-Ni(111)	Lee <i>et al.</i> [62]

<sup>a</sup> For further details please refer to the websites <https://wiki.fysik.dtu.dk/dacapo/>, <http://www.vasp.at/>, <http://www.uam.es/siesta/>, and <http://dft.sandia.gov/Quest/>. <sup>b</sup> PW91 (Perdew-Wang 91 functional [63]), RPBE (Revised Perdew-Burke-Ernzerhof functional [64]), PBE (Perdew-Burke-Ernzerhof functional [65]) and GGA (generalized gradient approximation). <sup>c</sup> PW-USPP (plane-wave for valence and ultrasoft pseudopotential for core electrons), PW-PAW (plane-wave for valence and projected augmented wave method for core electrons [66,67]), DZP-TMPP (double zeta plus polarization for valence and Troullier-Martins norm-conserving scalar relativistic pseudopotential for core). <sup>d</sup> Periodic slab models were employed to define the different Miller index surfaces. <sup>e</sup> Two rows were removed in the top layer of the Ru(001) and Re(001) surfaces for obtaining a stepped model surface.

On both surfaces the barriers calculated for the dissociation reactions described by Equation (2) (Fe, 1.96 eV; Co, 3.80 eV) and 3b (Fe, 1.63 eV; Co, 3.26 eV) are significantly larger than those calculated for reaction 4b (Fe, 0.79 eV; Co, 0.95 eV), *cf.* Table 2. Additionally, the barriers for formation of the HCO species (Equation (4a)) are smaller, on Fe(110), or identical, on Co(0001), to those leading to the

COH intermediate [19]. These results suggest that the breakage of the C–O bond occurs only after hydrogenation of the carbon atom of the CO species [19]. Using another computational code, Inderwildi *et al.* reported that the C–O bond dissociation from the formyl species was also much more favorable than the direct C–O bond breakage on Fe(111) [49], with values 1.17 eV (Equation 4b) and 1.76 eV (Equation (2)), and on Co(0001) [50], with values 1.00 eV (Equation 4b) and 2.82 eV (Equation (2)). A similar mechanistic profile for the dissociation of the C–O bond was obtained when the unity bond index-quadratic exponential potential (UBI-QEP) method [68] was applied to the synthesis of C<sub>1</sub>–C<sub>2</sub> alkanes or alkenes on Co [69].

**Table 2.** Activation energy barriers (eV) for the CO bond break through different reaction routes on several metallic surfaces <sup>a</sup>.

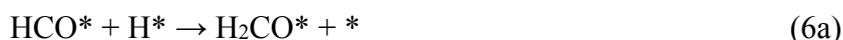
Reaction route	Fe(110)	Co(0001)	Fe(111)
CO* + * → C* + O*	1.96 [19]	3.80 [19]; 2.82 [50]	1.76 [49]
CO* + H* → COH* + * → C* + OH*	1.63 [19]	3.26 [19]	
CO* + H* → HCO* + * → CH* + O*	0.79 [19]	0.95 [19]; 1.00 [50]	1.17 [49]
HCO* + H* → HCOH* + * → CH* + OH*	0.65 [19]	1.10 [19]	
HCO* + H* → H <sub>2</sub> CO* + * → CH <sub>2</sub> * + O*	3.29 [19]	1.63 [19]	

<sup>a</sup> For reaction routes including several steps, the energy corresponds to the highest barrier along the route.

The decomposition of the formyl species (Equation (4b)) has to compete with further hydrogenation of the latter species to hydroxymethylene, HCOH, followed by its decomposition,



or leading to formaldehyde, H<sub>2</sub>CO, followed by its decomposition,



While the formation of the formaldehyde species appears to be possible [19], the cleavage of the C–O bond in the latter species seems to be prohibited, because reaction 6b has to surmount quite large energy barriers with values 3.29 eV on Fe(110) and 1.63 eV on Co(0001) [19]. Thus, the fate of formaldehyde will be one of the following: (i) decomposition into HCO and H surface species (reverse of reaction 6a); (ii) desorption from the surface; or (iii) further reaction to other oxygenated compounds, e.g., formate, HCOO, species. However, based on the DFT computed barrier for the reverse of reaction 6a on Co(0001), *i.e.*, 0.22 eV (0.13 eV with zero-point energy corrections) [70], formaldehyde desorption or further reaction to other oxygenated compounds seem difficult.

DFT-derived barriers for the reaction of Fischer-Tropsch synthesis on Ru catalysts show that CO predominantly reacts at (111) terraces through H-assisted reactions via the formyl route [51]. The formation of formyl species was experimentally detected by Eckle *et al.* [71] in time resolved *in situ* diffuse reflectance infrared Fourier transform spectroscopy (DRIFTS) measurements on Ru/Al<sub>2</sub>O<sub>3</sub> catalyst in idealized reformat (CO/H<sub>2</sub>/N<sub>2</sub>) conditions (band at 1760 cm<sup>-1</sup>). As it happens for Co and Fe, barriers on Ru catalysts for the unassisted reaction are much higher than those calculated after

hydrogenation; this is the case of CO dissociation on the planar (111) terraces and also on low-coordination atoms at step-edge sites. The latter conclusions contrast with results arising from DFT/PW91 studies by van Santen and co-workers, concerning the CO dissociation on stepped Ru(10 $\bar{1}$ 5) [52], and on open Ru(11 $\bar{2}$ 1) [53] or Ru(10 $\bar{1}$ 0)B [54] surfaces, where calculated barriers for CO direct dissociation on low-coordinated sites are only 0.92 eV, 0.67 eV and 0.49 eV, respectively. The barriers on these three Ru surfaces are significantly smaller than that calculated for the reaction on the planar Ru(0001) surface, *i.e.*, 2.35 eV [52]; such barriers are also smaller than those required to cleave the C–O bond via the hydroxymethylidyne or the formyl routes. The latter conclusions can be extended to Co based catalysts [54]. However, formation of formyl species is predicted on the Co(10 $\bar{1}$ 0)B surface but its decomposition seems to be unaffordable [54]. Interestingly, in the DRIFTS experiments of Eckle *et al.* [71] but on a Ru/zeolite catalyst, it was not observed the band at 1760 cm $^{-1}$  attributed to adsorbed HCO species. These results are strong evidences that quite small changes in the structure of a typical catalyst for the Fischer-Tropsch reaction can change dramatically its activity. Similar conclusions are attained from recent DFT/PBE calculations by Liu *et al.*, which demonstrate that the Fischer-Tropsch reaction on Co catalysts is structure sensitive [55]. In the case of the flat Co(0001) surface, the mechanism through the formyl intermediate is the most favorable while on Co surfaces possessing less coordinated atoms, the mechanism based on the direct CO dissociation on the surface is also feasible.

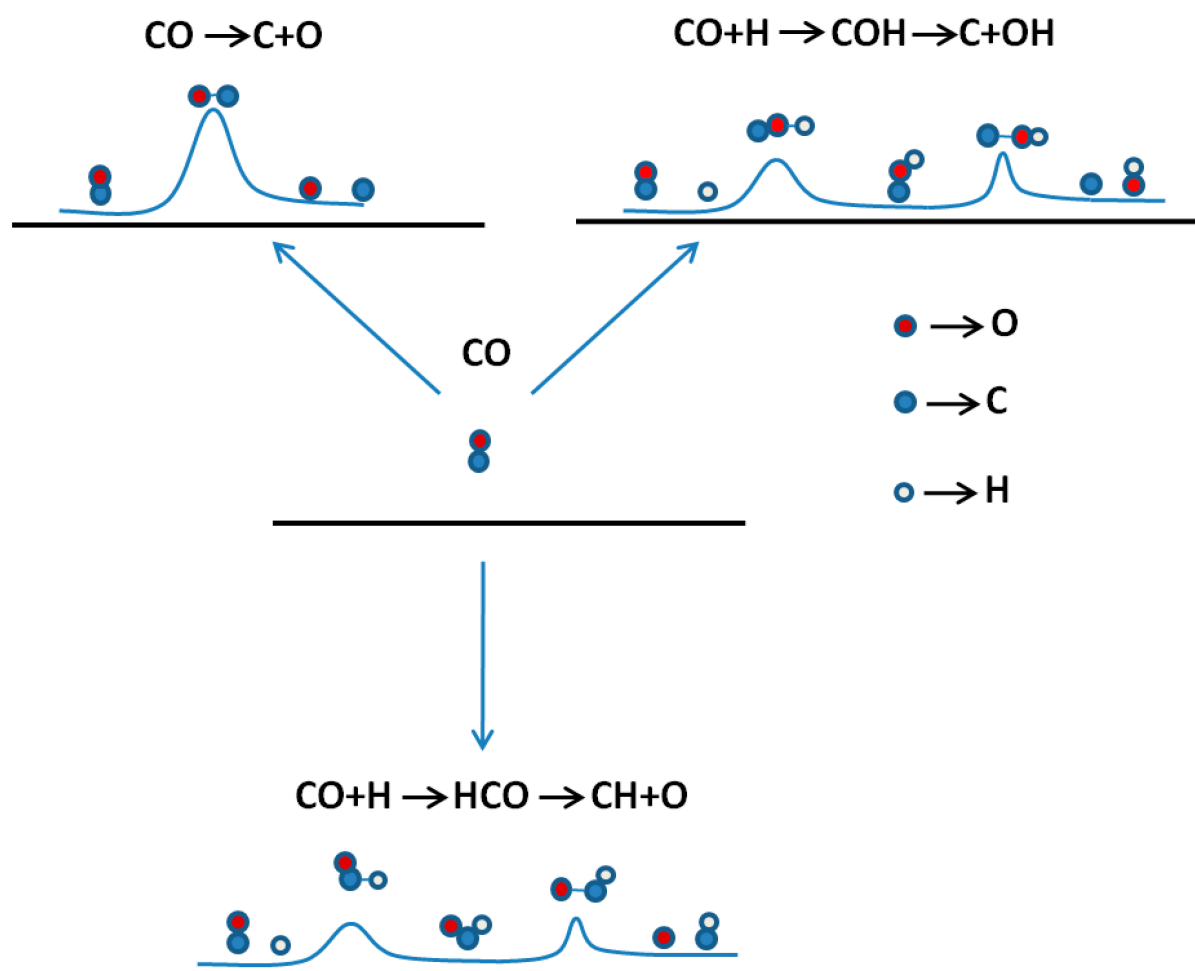
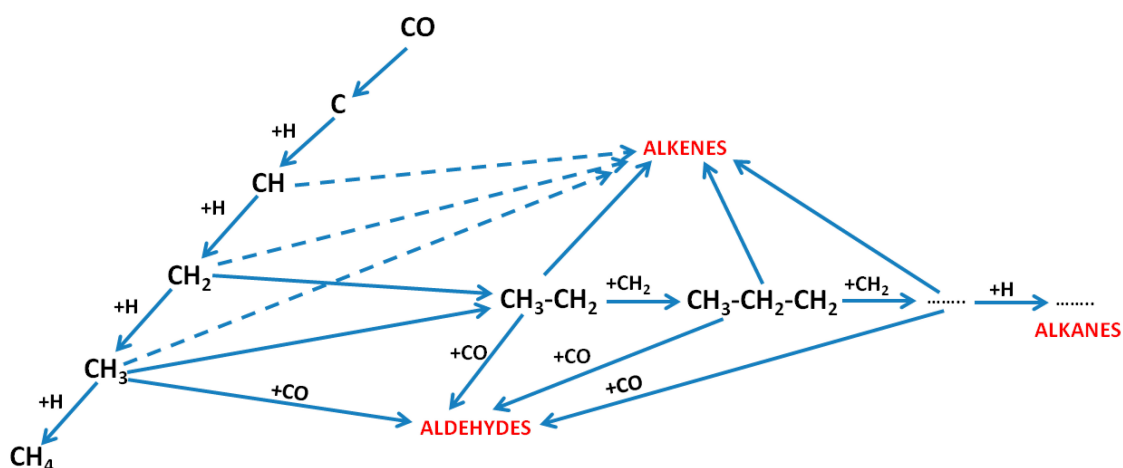


**Figure 1.** Representation of the carbide (**top left**), hydroxymethylidyne (**top right**) and formyl (**bottom**) routes for the CO dissociation in the Fischer-Tropsch reaction.

Recently, we considered the DFT/PW91 approach to study the mechanisms of methane and methanol formation on nickel based catalysts [56]. Nickel is active per se and has been found to promote the activity of iron and cobalt catalysts in the Fischer-Tropsch reaction [72] and references therein]. Therefore, it is not surprising to find in the literature several reports on the consideration of Ni-based catalysts for this reaction [73]. However, the number of studies with Ni-based catalysts is much smaller than with catalysts based on Co and Fe, maybe because the former catalysts are associated with formation of volatile carbonyls, which leads to deactivation and loss of the active phase [73]. As it happens in so many occasions, the catalyst formulation and the nature of the support seem to affect the conclusions about the influence of Ni species in the catalytic activity. In our computational study, our goal was to understand how the addition of a second metal (bimetallic catalyst) affect the activity of Ni in the Fischer-Tropsch synthesis reaction. With that aim we prepared flat (111) and crest (110) models of the Rh@Ni and Ru@Ni catalytic surfaces and compared the reaction mechanistic profiles on the latter with the profile calculated on a pure Ni surface [56]. We have found that surfaces possessing low coordinated atoms are more reactive than flat surfaces in the catalysis of dissociative reaction steps, which are in fact the rate determining steps of the process. Furthermore, it was found that the reactions toward methanol and methane formation preferentially evolve through the formyl intermediate on all the surfaces. Additionally, the reaction selectivity toward methane or methanol was affected by the surface doping and by the presence of low coordinated atoms on the surface. In fact, the routes leading toward methanol and methane on pure nickel surfaces and on flat surfaces doped with Rh or Ru atoms have similar activation energy barriers, while in the routes on crested doped surfaces the methane formation is more feasible than that of methanol [56].

DFT calculations were also used in studies of the mechanisms of hydrocarbon chain growth and chain termination, which are essential aspects in the synthesis of long chain hydrocarbons and oxygenated compounds through the Fischer-Tropsch process [57,58,74]. The reaction routes proposed are the carbide (also known as alkyl mechanism) and the CO insertion mechanisms, *cf.* Figure 2 [74]. In the carbide mechanism, the CO molecules dissociate to form  $\text{CH}_x$  intermediates. This process initiates the overall reaction, and the growth of the chains by reaction of these intermediates with other adsorbed  $\text{C}_n\text{H}_y$  intermediates eventually formed on the catalyst surface. In the CO insertion mechanism, the process is initiated by the formation of the  $\text{CH}_x$  species on the catalyst surface upon dissociation of CO, which is followed by (i) insertion of a CO molecule into the  $\text{CH}_x$  intermediate and by (ii) breakage of the CO bond in the resulting compound. This two-step mechanism will lead to the formation of long chain  $\text{C}_n\text{H}_y$  species. Thus, as it is well-illustrated in Figure 2, the chain growth in the carbide mechanism occurs through consecutive insertion of  $\text{CH}_x$  groups, while in the case of the CO insertion mechanism the chain growth occurs by sequential insertion of a CO molecule in  $\text{C}_n\text{H}_y$  species and cleavage of the inserted C–O bond. The reader must be aware of the mechanistic complexity of the Fischer-Tropsch process since, depending on the conditions, the reaction may go in the opposite direction, *i.e.*, to the steam reforming of alcohols or hydrocarbons [59,60,75], being Ni [76,77], Co [78–81], or Rh [78] the most common catalysts for the latter reaction. Although experimental knowledge acquired along the years allowed the proposal of different reaction routes, later analyses proved several of those to be less probable. An overview of such routes can be found in the work of Davis *et al.* [7].

## a) CARBIDE MECHANISM



## b) CO INSERTION MECHANISM

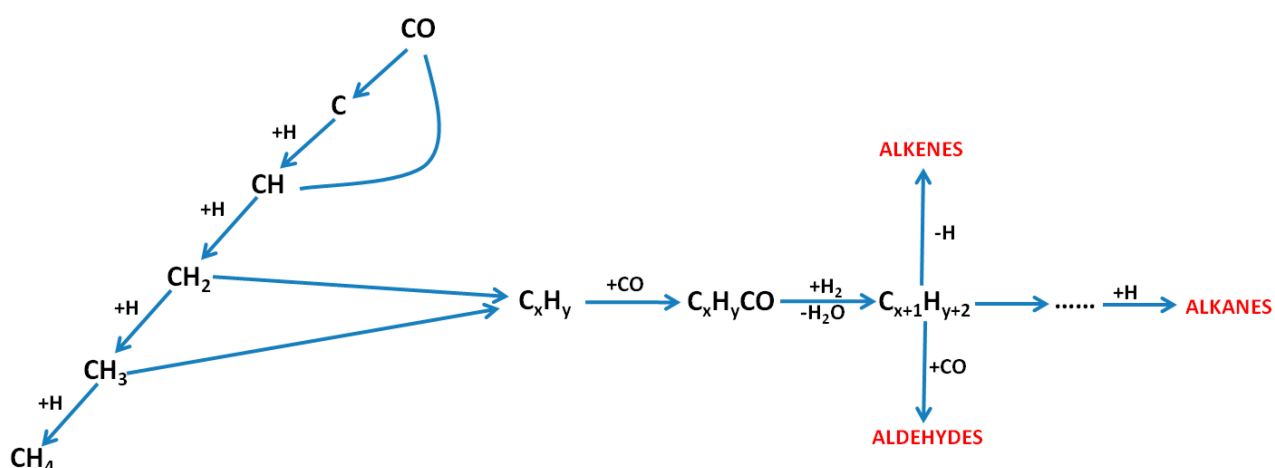


**Figure 2.** Representation of the Fischer-Tropsch (a) carbide and (b) CO insertion mechanisms steps (all the intermediates species represented are adsorbed on the surface).

Cheng *et al.* [57,58] investigated by DFT which are the  $\text{CH}_x$  intermediates that are preferentially coupled during the hydrocarbon chain growth on stepped Co, Rh, Ru, Fe and Re surfaces via the carbide mechanism. They found that despite the transition state structures are quite similar, the energy barriers for the different C–C coupling reactions differ considerably among the transition metals considered in their work, which leads to different preferential paths for the chain growth in each metal. In fact, C + CH and CH + CH paths are preferred on Ru and Rh, C +  $\text{CH}_3$  and  $\text{CH}_2$  +  $\text{CH}_2$  on Co, C +  $\text{CH}_3$  on Fe and C + CH on Re. Thus, with the exception of Ru and Rh surfaces, different coupling pathways are observed on different metal surfaces.

DFT calculations have been also used with success in the explanation of the catalyst deactivation by carbon deposition or sulfur [61,62,82]. Within such works, Zhang *et al.* [61] studied the co-adsorption of CO and S species on the Rh(111) surface and found that the chemisorption of each species is not significantly influenced by the chemisorption of the other species. Thus, they concluded that the interaction between the CO and S species co-adsorbed on the metal surface is mainly short range type and, therefore, the suggestion for the responsibility of the long range electronic effect in the reduction of the CO methanation in presence of S is very likely incorrect. Czekaj *et al.* [82] studied also the

poisoning of a Ni/ $\gamma$ -Al<sub>2</sub>O<sub>3</sub> catalyst by sulfur with the RPBE approach and cluster models. They found several sulfur containing species to be stable on the catalyst, both on the metallic particles and on the oxide support, as for example, carbonyl sulfide, hydrogen sulfide and hydrogen thiocarbonates. The high stability of the sulfur containing adsorbates was suggested to deactivate the catalyst. Lee *et al.* [62] investigated by DFT the effect of adding Ni in the improvement of the sulfur tolerance of a Rh catalyst for the reaction of CO dissociation. In their calculations, they compared the adsorption and dissociation of CO on bimetallic RhNi(111) catalysts having compositions Rh<sub>1</sub>Ni<sub>2</sub> and Rh<sub>2</sub>Ni<sub>1</sub> with those on pure Ni(111) and Rh(111) surfaces. They demonstrate that the CO dissociation is less affected by sulfur poison on the bimetallic catalyst than on pure rhodium. This was attributed to the effect of Ni on the bimetallic catalysts which mitigates the repulsion of the adsorbed sulfur with the transition state structure during the CO dissociation. In fact, the repulsion between the adsorbed sulfur and the stretched CO molecule leads to higher reaction barriers than on the clean rhodium surfaces [62]. In the case of Fischer-Tropsch reaction poisoning, DFT calculations allowed to explain the effect of the Pt and Ru promoters in the prevention of the Co catalyst deactivation by carbon deposition at the catalyst surface in the reaction of CO hydrogenation. Balakrishnan *et al.* [32] considered pure Co and bimetallic models, where Co atoms were replaced by Pt or Ru, and found that the presence of the promoters in the catalyst decreased the carbon hydrogenation barrier and increased the carbon-carbon coupling barrier, but without changing the barriers for the diffusion of C atoms. These authors also found that the effect of Pt in the destabilization of adsorbed carbon structures was more significant than that of Ru. Very recently, it was unraveled how carbon deposition (together with CO adsorbates) can affect the surface roughness (surface reconstruction) of Co catalysts [33].

### 3. Conclusions

In this review it was analyzed how the inclusion of additional components in the traditional catalysts for the Fischer-Tropsch reaction catalysis changes the preference for a specific reaction mechanism and how they influence the catalyst activity and selectivity.

It was analyzed the energetics of the dissociation of the C–O bond in carbon monoxide. Generally speaking, the density functional calculations suggest that the direct dissociation of CO is less feasible than the dissociation of the bond in the products of its hydrogenation, *i.e.*, hydroxymethyldyne (COH) or formyl (HCO) species. In most cases, the formation of the latter species is much easier and the dissociation of its C–O bond is the less costly. Nevertheless, the breakage of the C–O bond in the formyl species has to compete with the formation of hydroxymethylene (HCOH) or formaldehyde (H<sub>2</sub>CO) by further hydrogenation, and it was pointed out that the direct C–O bond rupture in CO competes with the dissociation of the bond in the formyl intermediate occurring on flat Co(0001) surfaces.

The chain growth was also explained with the aid of results from density functional theory calculations. Two alternative mechanisms, *i.e.*, the carbide and the CO insertion, arise as the most probable and are the most accepted nowadays. It is suggested that the occurrence of one or another is dramatically dependent on the nature of the catalyst and on the reaction conditions considered.

It was also reviewed the effects of poisoning and promoting species in the global catalytic activity by looking at the stability (energies of adsorption) of poisoning species such as sulfur containing molecules or carbon.

From what has been said above, the combination of density functional theory and realistic catalyst models provided very useful adsorption, diffusion, reaction and activation energies for the elementary steps in the Fischer-Tropsch process, which allowed the clarification of the preferential reaction mechanisms and also the understanding of atomic level structural details and their influence in the catalytic activity. Such information is crucial to design more efficient catalysts in the near future.

### Acknowledgments

Thanks are due to Fundação para a Ciência e Tecnologia (FCT), Lisbon, Portugal, and to FEDER for financial support to REQUIMTE (projects Pest-C/EQB/LA0006/2013 and NORTE-07-0124-FEDER-000067-NANOCHEMISTRY) and to CICECO (projects Pest-C/CTM/LA0011/2013 and FCOMP-01-0124-FEDER-037271) and for Programa Investigador FCT. This work has been supported also by FCT through project PTDC/QUI-QUI/117439/2010 (FCOMP-01-0124-FEDER-020977) co-financed by *Programa COMPETE*. JLCF acknowledges FCT for the grant SFRH/BPD/64566/2009 co-financed by the *Programa Operacional Potencial Humano (POPH)/Fundo Social Europeu (FSE)*; *Quadro de Referência Estratégico Nacional 2009–2013 do Governo da República Portuguesa*.

### Author Contributions

José L. C. Fajín and José R. B. Gomes conceived the outline of the review and selected the materials. All authors contributed to the writing of the paper.

### Conflicts of Interest

The authors declare no conflict of interest.

### References

1. Fischer, F.; Tropsch, H. Synthesis of petroleum at atmospheric pressures from gasification products of coal. *Brennst. Chem.* **1926**, *7*, 97–104.
2. Anderson, R.B. *The Fischer Tropsch Synthesis*; Academic Press: New York, NY, USA, 1984.
3. Kusama, H.; Okabe, K.; Arakawa, H. Characterization of Rh-Co/SiO<sub>2</sub> catalysts for CO<sub>2</sub> hydrogenation with TEM, XPS and FT-IR. *Appl. Catal. A* **2001**, *207*, 85–94.
4. Schulz, H. Major and minor reactions in Fischer-Tropsch synthesis on cobalt catalysts. *Top. Catal.* **2003**, *26*, 73–85.
5. Lögdberg, S.; Lualdi, M.; Järås, S.; Walmsley, J.C.; Blekkan, E.A.; Rytter, E.; Holmen, A. On the selectivity of cobalt-based Fischer-Tropsch catalysts: Evidence for a common precursor for methane and long-chain hydrocarbons. *J. Catal.* **2010**, *274*, 84–98.
6. Guzzi, L.; Stefler, G.; Koppány, Z.; Borkó, L. CO hydrogenation over Re-Co bimetallic catalyst supported over SiO<sub>2</sub>, Al<sub>2</sub>O<sub>3</sub> and NaY zeolite. *React. Kinet. Catal. Lett.* **2001**, *74*, 259–269.
7. Davis, B.H. Fischer-Tropsch synthesis: Current mechanism and futuristic needs. *Fuel Process. Technol.* **2001**, *71*, 157–166.
8. Tupabut, P.; Jongsomjit, B.; Praserttham, P. Impact of boron modification on MCM-41-supported cobalt catalysts for hydrogenation of carbon monoxide. *Catal. Lett.* **2007**, *118*, 195–202.

9. Dorner, R.W.; Hardy, D.R.; Williams, F.W.; Davis, B.H.; Willauer, H.D. Influence of gas feed composition and pressure on the catalytic conversion of CO<sub>2</sub> to hydrocarbons using a traditional cobalt-based Fischer-Tropsch catalyst. *Energ. Fuel.* **2009**, *23*, 4190–4195.
10. Rønning, M.; Tsakoumis, N.E.; Voronov, A.; Johnsen, R.E.; Norby, P.; van Beek, W.; Borg, Ø.; Rytter, E.; Holmen, A. Combined XRD and XANES studies of a Re-promoted Co/γ-Al<sub>2</sub>O<sub>3</sub> catalyst at Fischer-Tropsch synthesis conditions. *Catal. Today* **2010**, *155*, 289–295.
11. Bezemer, G.L.; Bitter, J.H.; Kuipers, H.P.C.E.; Oosterbeek, H.; Holewijn, J.E.; Xu, X.; Kapteijn, F.; van Dillen, A.J.; de Jong, K.P. Cobalt particle size effects in the Fischer-Tropsch reaction studied with carbon nanofiber supported catalysts. *J. Am. Chem. Soc.* **2006**, *128*, 3956–3964.
12. Wang, C.; Zhao, H.; Wang, H.; Liu, L.; Xiao, C.; Ma, D. The effects of ionic additives on the aqueous-phase Fischer-Tropsch synthesis with a ruthenium nanoparticle catalyst. *Catal. Today* **2012**, *183*, 143–153.
13. Inderwildi, O.R.; Jenkins, S.J. *In-silico* investigations in heterogeneous catalysis—Combustion and synthesis of small alkanes. *Chem. Soc. Rev.* **2008**, *37*, 2274–2309.
14. Stranges, A.N. A History of the Fischer-Tropsch Synthesis in Germany 1926–45. In *Fischer-Tropsch Synthesis, Catalysts, and Catalysis*, 1st ed.; Davis, B.H., Ocelli, M.L., Eds.; Elsevier B.V.: Amsterdam, The Netherlands, 2007; pp. 1–28.
15. Davis, B.H.; Ocelli, M.L. *Advances in Fischer-Tropsch Synthesis, Catalysts, and Catalysis*; CRC Press, Taylor & Francis Group: Boca Raton, FL, USA, 2010.
16. Jacquemin, M.; Beuls, A.; Ruiz, P. Catalytic production of methane from CO<sub>2</sub> and H<sub>2</sub> at low temperature: Insight on the reaction mechanism. *Catal. Today* **2010**, *157*, 462–466.
17. Park, S.-J.; Kim, S.-M.; Woo, M.H.; Bae, J.W.; Jun, K.-W.; Ha, K.-S. Effects of titanium impurity on alumina surface for the activity of Co/Ti–Al<sub>2</sub>O<sub>3</sub> Fischer-Tropsch catalyst. *Appl. Catal. A* **2012**, *419–420*, 148–155.
18. Nawdali, M.; Bianchi, D. The impact of the Ru precursor on the adsorption of CO on Ru/Al<sub>2</sub>O<sub>3</sub>: Amount and reactivity of the adsorbed species. *Appl. Catal. A* **2002**, *231*, 45–54.
19. Ojeda, M.; Nabar, R.; Nilekar, A.U.; Ishikawa, A.; Mavrikakis, M.; Iglesia, E. CO activation pathways and the mechanism of Fischer-Tropsch synthesis. *J. Catal.* **2010**, *272*, 287–297.
20. Gual, A.; Godard, C.; Castillon, S.; Curulla-Ferré, D.; Claver, C. Colloidal Ru, Co and Fe-nanoparticles. Synthesis and application as nanocatalysts in the Fischer-Tropsch process. *Catal. Today* **2012**, *183*, 154–171.
21. Senanayake, S.D.; Evans, J.; Agnoli, S.; Barrio, L.; Chen, T.-L.; Hrbek, J.; Rodriguez, J.A. Water-gas shift and CO methanation reactions over Ni-CeO<sub>2</sub>(111) catalysts. *Top. Catal.* **2011**, *54*, 34–41.
22. Bundhoo, A.; Schweicher, J.; Frennet, A.; Kruse, N. Chemical transient kinetics applied to CO hydrogenation over a pure nickel catalyst. *J. Phys. Chem. C* **2009**, *113*, 10731–10739.
23. Vendelbo, S.B.; Johansson, M.; Mowbray, D.J.; Andersson, M.P.; Abild-Pedersen, F.; Nielsen, J.H.; Nørskov, J.K.; Chorkendorff, I. Self blocking of CO dissociation on a stepped ruthenium surface. *Top. Catal.* **2010**, *53*, 357–364.
24. Williams, C.T.; Black, C.A.; Weaver, M.J.; Takoudis, C.G. Adsorption and hydrogenation of carbon monoxide on polycrystalline rhodium at high gas pressures *J. Phys. Chem. B* **1997**, *101*, 2874–2883.

25. Jenewein, B.; Fuchs, M.; Hayek, K. The CO methanation on Rh/CeO<sub>2</sub> and CeO<sub>2</sub>/Rh model catalysts: A comparative study. *Surf. Sci.* **2003**, 532–535, 364–369.
26. Bulushev, D.A.; Froment, G.F. A DRIFTS study of the stability and reactivity of adsorbed CO species on a Rh/ $\gamma$ -Al<sub>2</sub>O<sub>3</sub> catalyst with a very low metal content. *J. Mol. Catal. A* **1999**, 139, 63–72.
27. Panagiotopoulou, P.; Kondarides, D.I.; Verykios, X.E. Mechanistic aspects of the selective methanation of CO over Ru/TiO<sub>2</sub> catalyst. *Catal. Today* **2012**, 181, 138–147.
28. Karelovic, A.; Ruiz, P. Mechanistic study of low temperature CO<sub>2</sub> methanation over Rh/TiO<sub>2</sub> catalysts. *J. Catal.* **2013**, 301, 141–153.
29. Izquierdo, U.; Barrio, V.L.; Bizkarra, K.; Gutierrez, A.M.; Arraibi, J.R.; Gartzia, L.; Bañuelos, J.; Lopez-Arbeloa, I.; Cambra, J.F. Ni and Rh-Ni catalysts supported on zeolites L for hydrogen and syngas production by biogas reforming processes. *Chem. Eng. J.* **2014**, 238, 178–188.
30. Pirola, C.; Scavini, M.; Galli, F.; Vitali, S.; Comazzi, A.; Manenti, F.; Ghigna, P. Fischer-Tropsch synthesis: EXAFS study of Ru and Pt bimetallic Co based catalysts. *Fuel* **2014**, 132, 62–70.
31. Christensen, J.M.; Medford, A.J.; Studt, F.; Jensen, A.D. High pressure CO hydrogenation over bimetallic Pt-Co catalysts. *Catal. Lett.* **2014**, 144, 777–782.
32. Balakrishnan, N.; Joseph, B.; Bhethanabotla, V.R. Effect of Pt and Ru promoters on deactivation of Co catalysts by C deposition during Fischer-Tropsch synthesis: A DFT study. *Appl. Catal.* **2013**, 462–463, 107–115.
33. Weststrate, C.J.; Ciobîcă, I.M.; Saib, A.M.; Moodley, D.J.; Niemantsverdriet, J.W. Fundamental issues on practical Fischer-Tropsch catalysts: How surface science can help. *Catal. Today* **2014**, 228, 106–112.
34. Bambal, A.S.; Guggilla, V.S.; Kugler, E.L.; Gardner, T.H.; Dadyburjor, D.B. Poisoning of a silica-supported cobalt catalyst due to presence of sulfur impurities in syngas during Fischer-Tropsch synthesis: Effects of chelating agent. *Ind. Eng. Chem. Res.* **2014**, 53, 5846–5857.
35. Tian, D.; Liu, Z.; Li, D.; Shi, H.; Pan, W.; Cheng, Y. Bimetallic Ni-Fe total-methanation catalyst for the production of substitute natural gas under high pressure. *Fuel* **2013**, 104, 224–229.
36. Tada, S.; Kikuchi, R.; Takagaki, A.; Sugawara, T.; Oyama, S.T.; Satokawa, S. Effect of metal addition to Ru/TiO<sub>2</sub> catalyst on selective CO methanation. *Catal. Today* **2014**, 232, 16–21.
37. Wang, G.; Zhang, K.; Liu, P.; Hui, H.; Tan, Y. Synthesis of light olefins from syngas over Fe-Mn-V-K catalysts in the slurry phase. *J. Ind. Eng. Chem.* **2013**, 19, 961–965.
38. Xu, J.-D.; Zhu, K.-T.; Weng, X.-F.; Weng, W.-Z.; Huang, C.-J.; Wan, H.-L. Carbon nanotube-supported Fe-Mn nanoparticles: A model catalyst for direct conversion of syngas to lower olefins. *Catal. Today* **2013**, 215, 86–94.
39. Shi, B.; Wu, L.; Liao, Y.; Jin, C.; Montavon, A. Explanations of the formation of branched hydrocarbons during Fischer-Tropsch synthesis by alkylidene mechanism. *Top. Catal.* **2014**, 57, 451–459.
40. Pendyala, V.R.R.; Shafer, W.D.; Jacobs, G.; Davis, B.H. Fischer-Tropsch synthesis: Effect of reaction temperature for aqueous-phase synthesis over a platinum promoted Co/alumina catalyst. *Catal. Lett.* **2014**, 144, 1088–1095.

41. Jermwongratanachai, T.; Jacobs, G.; Shafer, W.D.; Pendyala, V.R.R.; Ma, W.; Gnanamani, M.K.; Hopps, S.; Thomas, G.A.; Kitiyanan, B.; Khalid, S.; *et al.* Fischer-Tropsch synthesis: TPR and XANES analysis of the impact of simulated regeneration cycles on the reducibility of Co/aluminacatalysts with different promoters (Pt, Ru, Re, Ag, Au, Rh, Ir). *Catal. Today* **2014**, *228*, 15–21.
42. Ning, W.; Yang, S.; Chen, H.; Yamada, M. Influences of K and Cu on coprecipitated FeZn catalysts for Fischer-Tropsch reaction. *Catal. Commun.* **2013**, *39*, 74–77.
43. Shimura, K.; Miyazawa, T.; Hanaoka, T.; Hirata, S. Factors influencing the activity of Co/Ca/TiO<sub>2</sub> catalyst for Fischer-Tropsch synthesis. *Catal. Today* **2014**, *232*, 2–10.
44. Azzam, K.; Jacobs, G.; Ma, W.; Davis, B.H. Effect of cobalt particle size on the catalyst intrinsic activity for Fischer-Tropsch synthesis. *Catal. Lett.* **2014**, *144*, 389–394.
45. Pendyala, V.R.R.; Jacobs, G.; Ma, W.; Klettlinger, J.L.S.; Yen, C.H.; Davis, B.H. Fischer-Tropsch synthesis: Effect of catalyst particle (sieve) size range on activity, selectivity, and aging of a Pt promoted Co/Al<sub>2</sub>O<sub>3</sub> catalyst. *Chem. Eng. J.* **2014**, *249*, 279–284.
46. Ding, M.; Qiu, M.; Liu, J.; Li, Y.; Wang, T.; Ma, L.; Wu, C. Influence of manganese promoter on co-precipitated Fe-Cu based catalysts for higher alcohols synthesis. *Fuel* **2013**, *109*, 21–27.
47. Bakar, W.A.W.A.; Ali, R.; Toemen, S. Catalytic methanation reaction over supported nickel-rhodium oxide for purification of simulated natural gas. *J. Nat. Gas Chem.* **2011**, *20*, 585–594.
48. Carencio, S.; Tuxen, A.; Chintapalli, M.; Pach, E.; Escudero, C.; Ewers, T.D.; Jiang, P.; Borondics, F.; Thornton, G.; Alivisatos, A.P.; *et al.* Dealloying of cobalt from CuCo nanoparticles under Syngas exposure. *J. Phys. Chem. C* **2013**, *117*, 6259–6266.
49. Inderwildi, O.R.; Jenkins, S.J.; King, D.A. Mechanistic studies of hydrocarbon combustion and synthesis on noble metals. *Angew. Chem. Int. Ed.* **2008**, *47*, 5253–5255.
50. Inderwildi, O.R.; Jenkins, S.J.; King, D.A. Fischer-Tropsch mechanism revisited: Alternative pathways for the production of higher hydrocarbons from synthesis gas. *J. Phys. Chem. C* **2008**, *112*, 1305–1307.
51. Loveless, B.T.; Buda, C.; Neurock, M.; Iglesia, E. CO chemisorption and dissociation at high coverages during CO hydrogenation on Ru catalysts. *J. Am. Chem. Soc.* **2013**, *135*, 6107–6121.
52. Ciobica, I. M.; van Santen, R.A. Carbon monoxide dissociation on planar and stepped Ru(0001) surfaces. *J. Phys. Chem. B* **2003**, *107*, 3808–3812.
53. Shetty, S.; Jansen, A.P.J.; van Santen, R.A. Direct versus hydrogen-assisted CO dissociation. *J. Am. Chem. Soc.* **2009**, *131*, 12874–12875.
54. Shetty, S.; Jansen, A.P.J.; van Santen, R.A. Hydrogen induced CO activation on open Ru and Co surfaces. *Phys. Chem. Chem. Phys.* **2010**, *12*, 6330–6332.
55. Liu, J.-X.; Su, H.-Y.; Li, W.-X. Structure sensitivity of CO methanation on Co (0001), (10 $\bar{1}$ 2) and (11 $\bar{2}$ 0) surfaces: Density functional theory calculations. *Catal. Today* **2013**, *215*, 36–42.
56. Fajín, J.L.C.; Cordeiro, M.N.D.S.; Gomes, J.R.B. Methanation of CO on pure and Rh or Ru doped nickel surfaces. *J. Phys. Chem.* **2014**, submitted.
57. Cheng, J.; Hu, P.; Ellis, P.; French, S.; Kelly, G.; Lok, C.M. A DFT study of the chain growth probability in Fischer-Tropsch synthesis. *J. Catal.* **2008**, *257*, 221–228.

58. Cheng, J.; Hu, P.; Ellis, P.; French, S.; Kelly, G.; Lok, C.M. Chain growth mechanism in Fischer-Tropsch synthesis: A DFT study of C-C coupling over Ru, Fe, Rh, and Re surfaces. *J. Phys. Chem. C* **2008**, *112*, 6082–6086.
59. Van Grootel, P.W.; Hensen, E.J.M.; van Santen, R.A. The CO formation reaction pathway in steam methane reforming by rhodium. *Langmuir* **2010**, *26*, 16339–16348.
60. Mueller, J.E.; van Duin, A.C.T.; Goddard III, W.A. Structures, energetics, and reaction barriers for CH<sub>x</sub> bound to the nickel (111) surface. *J. Phys. Chem. C* **2009**, *113*, 20290–20306.
61. Zhang, C.J.; Hu, P.; Lee, M.-H. A density functional theory study on the interaction between chemisorbed CO and S on Rh(111). *Surf. Sci.* **1999**, *432*, 305–315.
62. Lee, K.; Song, C.; Janik, M.J. Density functional theory study of sulfur tolerance of CO adsorption and dissociation on Rh-Ni binary metals. *Appl. Catal. A* **2010**, *389*, 122–130.
63. Perdew, J.P.; Chevary, J.A.; Vosko, S.H.; Jackson, K.A.; Pederson, M.R.; Singh, D.J.; Fiolhais, C. Atoms, molecules, solids, and surfaces: Applications of the generalized gradient approximation for exchange and correlation. *Phys. Rev. B* **1992**, *46*, 6671–6687.
64. Hammer, B.; Hansen, L.B.; Nørskov, J.K. Improved adsorption energetics within density-functional theory using revised Perdew-Burke-Ernzerhof functionals. *Phys. Rev. B* **1999**, *59*, 7413–7421.
65. Perdew, J.P.; Burke, K.; Ernzerhof, M. Generalized gradient approximation made simple. *Phys. Rev. Lett.* **1996**, *67*, 3865–3868.
66. Blöchl, P.E. Projector augmented-wave method. *Phys. Rev. B* **1994**, *50*, 17953–17979.
67. Kresse, G.; Joubert, D. From ultrasoft pseudopotentials to the projector augmented-wave method. *Phys. Rev. B* **1999**, *59*, 1758–1775.
68. Shustorovich, E.; Sellers, H. The UBI-QEP method: A practical theoretical approach to understanding chemistry on transition metal surfaces. *Surf. Sci. Rep.* **1998**, *31*, 1–119.
69. Storsæter, S.; Chen, D.; Holmen, A. Microkinetic modelling of the formation of C1 and C2 products in the Fischer-Tropsch synthesis over cobalt catalysts. *Surf. Sci.* **2006**, *600*, 2051–2063.
70. Luo, W.; Asthagiri, A. Density functional theory study of methanol steam reforming on Co(0001) and Co(111) surfaces. *J. Phys. Chem. C* **2014**, *118*, 15274–15285.
71. Eckle, S.; Anfang, H.-G.; Behm, R.J. Reaction intermediates and side products in the methanation of CO and CO<sub>2</sub> over supported Ru catalysts in H<sub>2</sub>-rich reformat gases. *J. Phys. Chem. C* **2011**, *115*, 1361–1367.
72. Li, T.; Wang, H.; Yang, Y.; Xiang, H.; Li, Y. Study on an iron-nickel bimetallic Fischer-Tropsch synthesis catalyst. *Fuel Proc. Technol.* **2014**, *118*, 117–124.
73. Enger, B.C.; Holmen, A. Nickel and Fischer-Tropsch synthesis. *Catal. Rev.: Sci. Eng.* **2012**, *54*, 437–488.
74. Van Santen, R.A.; Markvoort, A.J.; Filot, I.A.W.; Ghouri, M.M.; Hensen, E.J.M. Mechanism and microkinetics of the Fischer-Tropsch reaction. *Phys. Chem. Chem. Phys.* **2013**, *15*, 17038–17063.
75. Birot, A.; Epron, F.; Descorme, C.; Duprez, D. Ethanol steam reforming over Rh/Ce<sub>x</sub>Zr<sub>1-x</sub>O<sub>2</sub> catalysts: Impact of the CO–CO<sub>2</sub>–CH<sub>4</sub> interconversion reactions on the H<sub>2</sub> production. *Appl. Catal. B* **2008**, *79*, 17–25.
76. Lv, X.; Chen, J.-F.; Tan, Y.; Zhang, Y. A highly dispersed nickel supported catalyst for dry reforming of methane. *Catal. Commun.* **2012**, *20*, 6–11.

77. Freni, S.; Cavallaro, S.; Mondello, N.; Spadaro, L.; Frusteri, F. Production of hydrogen for MC fuel cell by steam reforming of ethanol over MgO supported Ni and Co catalysts. *Catal. Commun.* **2003**, *4*, 259–268.
78. Karim, A.M.; Su, Y.; Sun, J.; Yang, C.; Strohm, J.J.; King, D.L.; Wang, Y. A comparative study between Co and Rh for steam reforming of ethanol. *Appl. Catal. B* **2010**, *96*, 441–448.
79. Lin, S.S.-Y.; Kim, D.H.; Ha, S.Y. Hydrogen production from ethanol steam reforming over supported cobalt catalysts. *Catal. Lett.* **2008**, *122*, 295–301.
80. Batista, M.S.; Santos, R.K.S.; Assaf, E.M.; Assaf, J.M.; Ticianelli, E.A. Characterization of the activity and stability of supported cobalt catalysts for the steam reforming of ethanol. *J. Power Sources* **2003**, *124*, 99–103.
81. Batista, M.S.; Santos, R.K.S.; Assaf, E.M.; Assaf, J.M.; Ticianelli, E.A. High efficiency steam reforming of ethanol by cobalt-based catalysts. *J. Power Sources* **2004**, *134*, 27–32.
82. Czekaj, I.; Struis, R.; Wambach, J.; Biollaz, S. Sulphur poisoning of Ni catalysts used in the SNG production from biomass: Computational studies. *Catal. Today* **2011**, *176*, 429–432.

© 2015 by the authors; licensee MDPI, Basel, Switzerland. This article is an open access article distributed under the terms and conditions of the Creative Commons Attribution license (<http://creativecommons.org/licenses/by/4.0/>).